Mean airflow patterns upwind of topographic obstacles and their implications for the formation of echo dunes: A wind tunnel simulation of the effects of windward slope

Guangqiang Qian,[1] Zhibao Dong,[1] Wanyin Luo,[1] and Junfeng Lu[1]

Received 4 March 2011; revised 2 August 2011; accepted 6 October 2011; published 9 December 2011.

[1] Secondary airflow plays an important role in dune formation and development. In the case of the echo dunes that form upwind of an obstacle, it introduces considerable complexity because both the initiation and development processes are influenced by airflow patterns. In this study, we measured the variations of airflow in front of obstacles with different windward (stoss) slope angles by means of particle-image velocimetry in a series of wind tunnel tests. The windward slope angle was the key factor in determining the secondary airflow patterns. The horizontal velocities decreased and the vertical velocities increased as the airflow approached perpendicular to the obstacle, and a vortex of reversed flow formed in front of obstacles with a stoss slope of 60° or steeper. The positions of airflow separation and of the core of the reversed vortex were a function of the windward slope angle. Depending on the position of the reverse vortex and its significance for the formation of echo dunes, the windward slope could be divided into three groups (65° or less, 70°–75°, and 80° or more). The horizontal velocity profiles deviated from a log linear distribution, resulting in five airflow regions with different rates of change of horizontal velocity. We discuss the significance of these velocity variations for sand accumulation and the effects of each airflow region on echo dune formation.

Citation: Qian, G., Z. Dong, W. Luo, and J. Lu (2011), Mean airflow patterns upwind of topographic obstacles and their implications for the formation of echo dunes: A wind tunnel simulation of the effects of windward slope, *J. Geophys. Res.*, *116*, F04026, doi:10.1029/2011JF002020.

1. Introduction

[2] Aeolian dunes can be categorized into three primary groups according to their method of initiation, although the names differ among classification systems: self-accumulated (autogenic) dunes and vegetation- and topography-influenced dunes [*Cooke et al.*, 1993; *Lancaster*, 1995; *Livingstone and Warren*, 1996; *Pye and Tsoar*, 2009]. Self-accumulated dunes, such as transverse dunes, linear dunes, and star dunes, are found in most sand seas, particularly where vegetation and topography do not influence the wind's flow patterns. Vegetation-influenced dunes, such as parabolic dunes, vegetated linear dunes, and nebkha dunes, develop in deserts where the precipitation or groundwater are sufficient for plants to survive. Dune accumulations associated with topographic obstacles can be divided into echo dunes that form upwind of an obstacle under the influence of reversed airflow, climbing dunes that form on the windward (stoss) side of a topographic obstacle, lee and shadow dunes and falling dunes that form on the leeward side of the topographic obstacle, and cliff-top dunes that form just downwind of the crest of an escarpment [*Tsoar*, 1983; *Howard*, 1985].

[3] Most types of self-accumulated and vegetated dunes have been documented, and there is now general consensus on their formation and development processes [*Lancaster*, 1995; *Livingstone et al.*, 2007]. However, dunes related to topographic obstacles have attracted less attention because of their comparatively limited distribution. In recent decades, the overexploitation of natural resources and construction of roads and other transportation infrastructure in deserts and the surrounding regions have led to significant aeolian erosion problems and a growing need for the prevention of the associated sand hazards. Human structures such as buildings, steep embankments, and sand-prevention fences resemble topographic obstacles, thus drifting sands can deposit around them and form echo dunes in front of the obstacle or can bury the structure as the sands climb the windward side and spillover onto the leeward side. Similar aeolian accumulations (such as climbing and falling dunes) have been found on Mars [*Chojnacki et al.*, 2010]; hence, a thorough investigation of their analogs on Earth will provide basic information for interpreting both terrestrial and extraterrestrial aeolian phenomena. Therefore, the study of topographic dunes has both theoretical and practical significance.

[4] Topographic dunes, and particularly climbing and falling dunes, may comprise large volumes of sand and may typically develop in relation to large topographic features

[1]Key Laboratory of Desert and Desertification, Cold and Arid Regions Environmental and Engineering Research Institute, Chinese Academy of Sciences, Gansu, China.

0148-0227/11/2011JF002020

Figure 1. Echo dunes can form upwind of a variety of topographic obstacles.

[*Evans*, 1962; *Lancaster and Tchakerian*, 1996]. However, echo dunes can form in front of small obstacles during a storm or as a result of strong winds over a long period of time [*Hesp et al.*, 2009]. Our field investigations of echo dunes have revealed that they can form in front of solid or porous obstacles such as small escarpments, buildings, yardangs, and sand-prevention fences (Figure 1). Most of them form in desert margins or in desertified areas that have an insufficient sediment supply to produce larger structures such as climbing dunes. Therefore, echo dunes are more common than larger topographic dunes in these areas, and understanding their formation has great practical significance for the protection of human structures.

[5] Since the 1940s, a number of hypotheses have been proposed to describe such accumulations in front of obstacles. *Bagnold* [1941] proposed that the initiation of echo dune formation resulted from saltating sand striking a vertical obstacle and that the rebounding grains deposited in front of the obstacle. *Petrov* [1962] suggested that the reflection of airflow in front of an obstacle, combined with the collision effect described by *Bagnold* [1941], accounted for their formation. However, *Embleton et al.* [1979] proposed that echo dunes were generated by a standing vortex. Currently, the most widely accepted and cited hypothesis for the formation of echo dunes was proposed by *Tsoar* [1983]. On the basis of the results of detailed wind tunnel tests, *Tsoar* [1983] proposed that a certain minimum angle of the windward slope was required for airflow separation and the generation of secondary airflow structures in front of solid obstacles, and that the effects of the resulting reverse vortex were important for echo dune formation. Recently, *Liu et al.* [1999] studied the processes involved in sand accumulation in front of various scale models of mountains that had a range of combinations of windward slope angle and incident wind direction in wind tunnel simulations and found that the maximum slope for the formation of climbing dunes or the minimum slope for the formation of echo dunes varied and decreased with increasing angle of incidence.

[6] These previous studies provided insights into the formation mechanisms of echo dunes. However, improvements in research on the dynamic processes involved in dune development and evolution, particularly with reference to self-accumulated dunes, have provided insights that are applicable to the formation of topography-influenced dunes. The secondary airflow induced by feedbacks between the bed form and the sand-bearing airflow is now considered to play an important role in the morphological and dynamic processes responsible for self-accumulated dunes [*Lancaster*, 1995; *Frank and Kocurek*, 1996; *Wiggs et al.*, 1996; *Walker*, 1999; *Wiggs*, 2001; *Walker and Nickling*, 2002; *Dong et al.*, 2007]. However, it would not be appropriate to directly apply the models of secondary airflow that have been developed for self-accumulated dunes to the processes of echo dune formation because the characteristics of the two

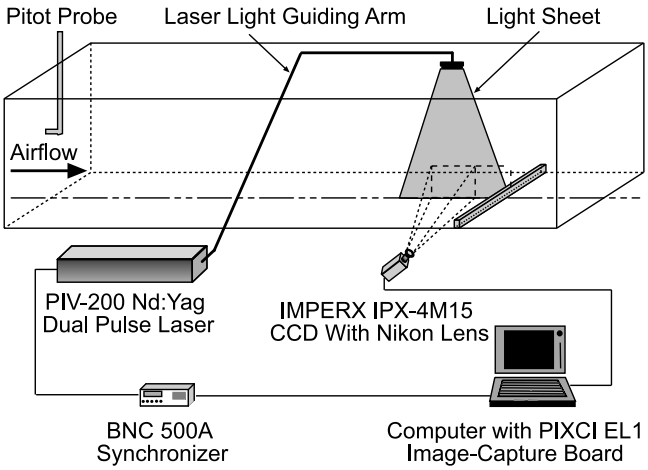

Figure 2. Illustration of the wind tunnel and measuring equipment used during the tests.

dunes are different. For self-accumulated dunes, the secondary airflow develops when the dune protrudes into the atmospheric boundary layer and becomes an obstacle for the airflow, whereas echo dunes are controlled by secondary airflow right from the start of their development because sand accumulation results from interactions between the free-stream airflow and a topographic obstacle. On the other hand, the self-accumulated dunes can interact with the secondary airflow and can deform as a result of this interaction because they consist of a mobile substrate, whereas echo dunes will achieve an equilibrium state under such flow patterns. As *Tsoar* [1983] also noted, growth of an echo dune will introduce more complexity into the evolution of the dune because of the superimposition of a dune-induced secondary airflow and the reversed airflow that develops in front of the obstacle. The effects of secondary airflow on echo dune formation and development have not been explored thoroughly until recently because of limitations on both the measuring equipment and the available theory. Hence, it is necessary to develop more precise instruments that can be used to generate high-quality data that can be combined with a theory of secondary airflow to interpret the dynamical processes responsible for the formation of echo dunes.

[7] The objectives of this study were to measure the secondary airflow in front of solid obstacles with different windward slopes and to discuss the significance of the resulting airflow patterns for the formation and development of echo dunes.

2. Wind Tunnel Experiments

[8] Our wind tunnel tests were carried out at the Key Laboratory of Desert and Desertification, Chinese Academy of Sciences. The indoor, blow-type, noncirculating wind tunnel has a total length of 10.5 m, with a 4 m test section; the cross section is 0.4 m in height and 0.4 m in width. The wind velocity can be adjusted continuously from 1 to 35 m s^{-1}. By introducing a series of roughness arrays at the entrance of the test section, the boundary layer thickness in the test section develops to a height of more than 120 mm.

[9] *Tsoar* [1983] found that echo dunes form in front of solid obstacles because of the effects of a reverse vortex that forms when the windward slope is steeper than 55°. Instead, at lower angles, climbing dunes develop. To permit an extensive comparison of secondary airflows in front of obstacles using more modern research tools, we constructed 12 wooden models with windward slope angles ranging between 35° and 90°, at intervals of 5°. The models were 25 mm tall and 400 mm wide and therefore occupied the whole width of the wind tunnel. The wood models were fixed perpendicular to the direction of the incident wind, 3.0 m downwind from the entrance of the test section. We used three free-stream wind velocities (U_f = 6, 8, and 10 m s^{-1}), measured 0.2 m above the floor immediately downwind of the entrance of the test section using a pitot tube. The Reynolds numbers ranged from 5.0×10^4 to 8.2×10^4 and therefore met the requirement of "Reynolds number independence" proposed by *White* [1996] for solid models. Figure 2 shows the layout of the wind tunnel and of the measuring equipment during our tests.

[10] The airflow velocities were measured using a particle-image velocimetry (PIV) system, which was provided by the Beijing Cubic World Science and Technology Development Co., Ltd. It has four main components: a dual-pulsed Nd:Yag laser with a guiding arm to generate a light sheet, a charge-coupled device (CCD) (Model IPX-4M15; Imperx Incorporated, Boca Raton, Florida) with a Nikon lens to capture images, a computer with an image-capture board to acquire and save the images, and a synchronizer to control the frequency of the laser and the CCD camera. To measure the wind velocities in front of obstacles using the PIV system, we installed an oil droplet generator (Model 9307–6; TSI Incorporated, Shoreview, Minnesota) at the entrance of the wind tunnel to generate small droplets (olive oil with a mean droplet size of 1 μm) as the tracer particles. After traveling 3 m, the particles had mixed with the air sufficiently well that their velocities could be used to represent the velocity of the airflow. The CCD's resolution was 2048 × 2048 pixels; with a scale of 0.05108 mm/pixel, its field of view is thus 104.6 × 104.6 mm when the camera is positioned 0.25 m from the laser light sheet. Capturing images of the flow field at two positions (the dashed rectangles in Figure 2) covered a total length of 209 mm. With a 5 Hz dual-pulse laser frequency, the camera can capture 10 frames (5 pairs) per second. We captured 200 frame pairs at each measurement position during a period of 40 s. Using a cross-correlation algorithm for each frame pair provides a data set for that image. The final measurement results thus represent an average of 200 data sets per wind speed. For more details about the calculation principle, refer to *Adrian* [1991] and *Raffel et al.* [2007].

[11] In this paper, we focus on the secondary airflow patterns that developed in front of the models at a free-stream wind velocity of 8 m s^{-1} because there were only slight variations in our results among the different wind velocities. To facilitate comparisons between this study and previous studies, we have normalized all measured velocities by dividing them by the free-stream wind velocity.

3. Results and Discussion

3.1. Velocity Contours

[12] Previous studies of dune dynamics within the atmospheric boundary layer have demonstrated that the airflow accelerated over the stoss slope of a transverse dune and

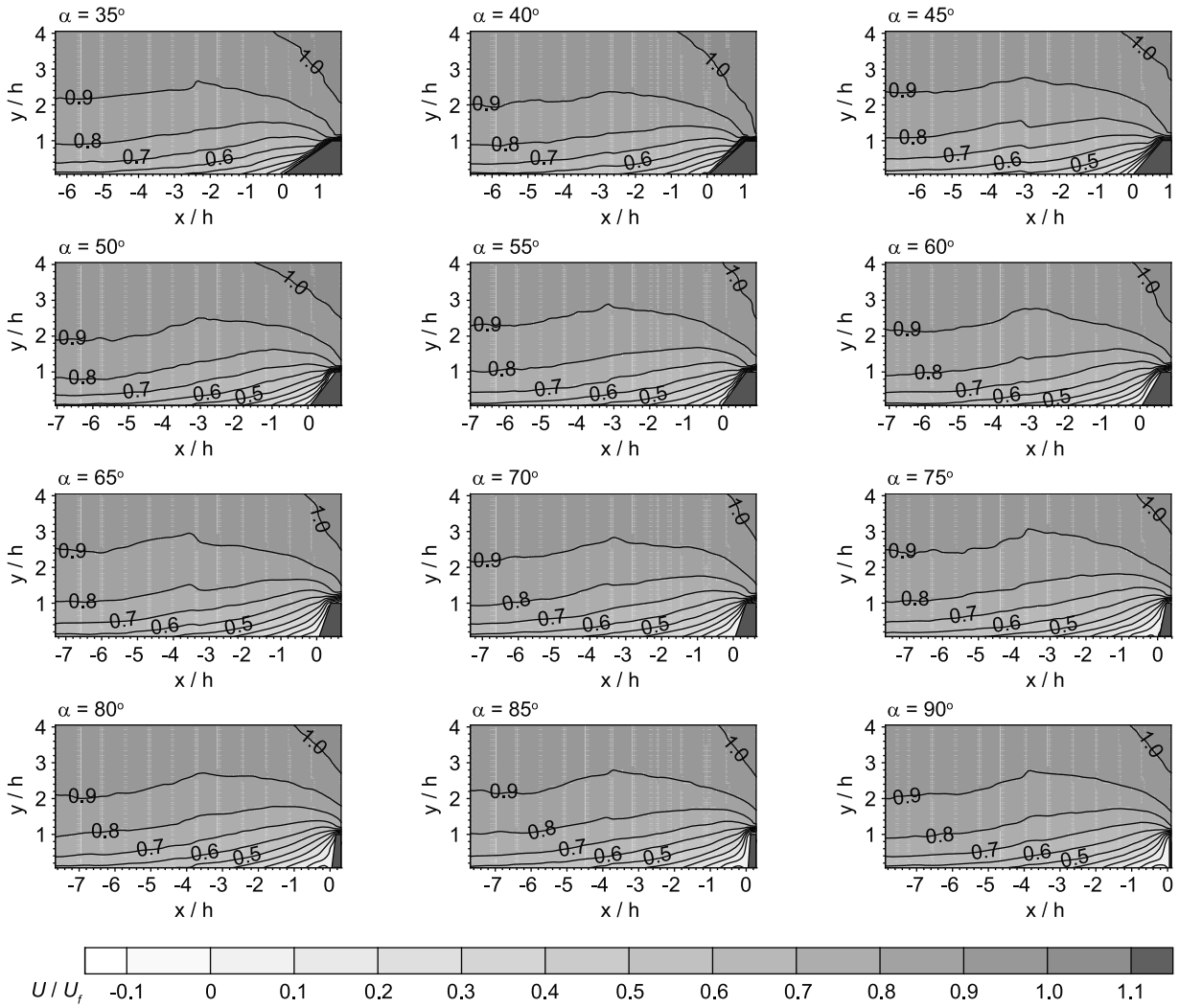

Figure 3. Contour maps of the variation in the dimensionless horizontal velocity as a function of windward slope angles. All measured wind velocities are expressed relative to the free-stream wind velocity of 8 m s^{-1} used in this study. All distances above the surface (y) and before and after the model (x) are expressed as multiples of h, the height of the model. U, horizontal wind speed; U_f, free-stream wind velocity.

decelerated in front of a steep obstacle such as an escarpment [*Bowen and Lindley*, 1977; *Emeis et al.*, 1995; *Lancaster et al.*, 1996; *Wiggs et al.*, 1996; *Weng et al.*, 2000; *Walker and Nickling*, 2003; *Lubitz and White*, 2007; *Qian et al.*, 2009]. The wind velocities measured by the PIV in this study also behaved differently when they approach solid obstacles with different slopes. Figures 3 and 4 show the variations in horizontal and vertical velocities as a function of the windward slope.

[13] Figure 3 reveals two obvious characteristics of the flow patterns: deceleration of the airflow (decreasing horizontal velocities) as the wind approaches the obstacle and the development of a reversed flow in front of steep obstacles. The decrease in horizontal velocities occurred farther from the obstacles for windward slope angles less than or equal to 55°, and clear reverse eddies developed upwind of the steeper obstacles. In contrast, vertical velocities increased as the airflow approached the obstacles (Figure 4). The direction of the vertical airflow changed from upward to downward in front of obstacles with a windward slope angle of 60° or more. These secondary airflow patterns indicate that flow separation occurred, leading to the formation of a reverse flow vortex in front of the obstacles when the windward slope angle increased to 60° or more. These results agree with the proposed minimum windward slope angle for sand accumulation proposed by *Tsoar* [1983]. *Tsoar* [1983] and *Liu et al.* [1999] found that the accumulation of sands and the formation of an echo dune upwind of an obstacle were determined by the flow separation and the formation of a reverse vortex upwind of the obstacle. Figures 3 and 4 also show that the ratios between the secondary airflow velocity and the free-stream wind velocity (i.e., the dimensionless velocities) varied with the angle of the windward slope, with the distance from the toe of the obstacle's stoss (windward) side, and with the height above the ground. In the remainder of section 3, we will discuss these patterns quantitatively.

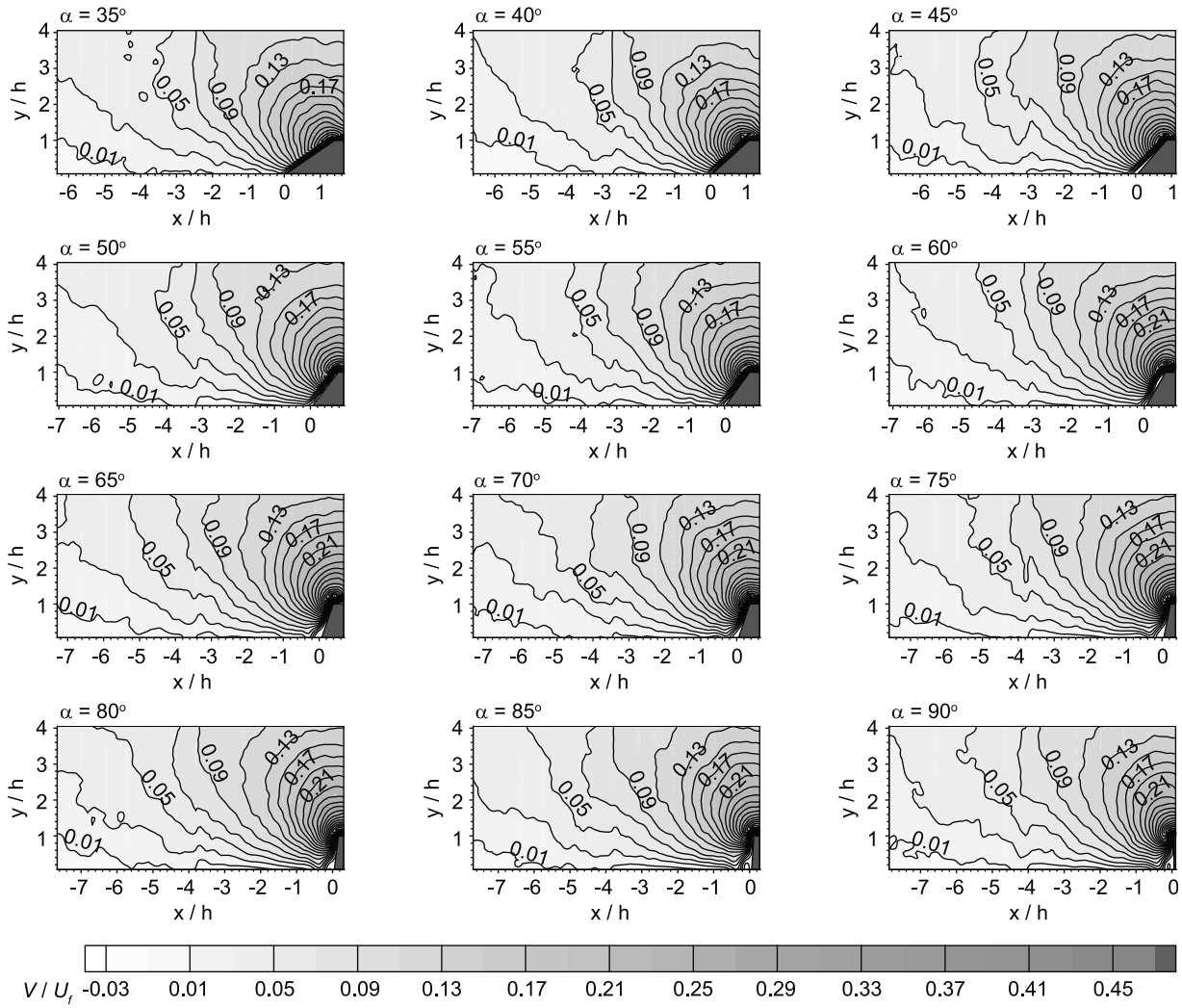

Figure 4. Contour maps of the dimensionless vertical velocity as a function of windward slope angles. All measured wind velocities are expressed relative to the free-stream wind velocity of 8 m s^{-1} used in this study. All distances above the surface (y) and before and after the model (x) are expressed as multiples of h, the height of the model. V, vertical wind speed; U_f, free-stream wind velocity.

3.2. Variations in the Velocity Components

[14] Table 1 summarized the variations in horizontal and vertical velocities at different heights in front of four typical obstacles. The changes of horizontal velocities show that deceleration only occurred near the ground (beneath a height of 1.0h, where h is the model height); otherwise, velocity decreased at greater distances but increased when the obstacle is approached at a height of 2.0h. These results show that the influence of a topographic obstacle on the approaching wind occurs closer to the near-surface layer (i.e., at a height less than that of the obstacle), which is where echo dunes form. The minimum value of horizontal velocity was negative (i.e., a reverse airflow) at a height of 0.07h and at stoss angles 55° or steeper. Table 1 also indicates that the reverse airflow disappeared completely at a height of 0.6h.

[15] The magnitude and rate of the deceleration of horizontal velocity were clearly influenced by the windward slope angle. The steeper windward slopes produced faster deceleration of horizontal velocity and a greater distance in which airflow stagnation occurred (Table 1). Nevertheless, these effects were most obvious near the ground and decreased in magnitude with increasing height. Although there was only a slight effect of airflow above 1.0h on the conditions required for the formation of echo dunes, we also saw acceleration of horizontal velocity at a height of 2.0h because the distinctive characteristics of the obstacle would affect the climbing of sand along a gentle windward slope. Beneath a height of 1.0h, the deceleration and reversal of airflow in the near-surface region in front of a topographic obstacle would decrease the ability of the airflow to carry sand, leading to the deposition of sand before the obstacle to form an echo dune near where the reverse vortex forms.

[16] *Tsoar*'s [1983] wind tunnel tests showed similar deceleration of horizontal velocity in front of inclined obstacles. Figure 5 shows the horizontal velocities at the lowest height (0.07h above the ground) measured by the PIV in this study and the results of the longitudinal (horizontal) velocity component measured by *Tsoar* [1983] using a hot-wire anemometer. The dimensionless velocities have a

Table 1. Variations in Horizontal and Vertical Velocities at Different Heights in Front of Four Typical Obstacles

Windward Slope	Height (y/h)	Dimensionless Velocity	Distance From Stoss Toe (x/h)									
			$-7h$	$-6h$	$-5h$	$-4h$	$-3h$	$-2h$	$-1h$	$-0.5h$	$-0.1h$	$0h$
50°	$0.07h$	U/U_f	0.589	0.581	0.576	0.540	0.466	0.415	0.304	0.196	0.152	0.089
	$0.07h$	V/U_f	0.000	0.002	0.003	0.009	0.009	0.011	0.018	0.025	0.028	0.014
	$0.6h$	U/U_f	0.759	0.754	0.740	0.714	0.676	0.621	0.558	0.493	0.416	0.404
	$0.6h$	V/U_f	0.004	0.011	0.017	0.028	0.035	0.057	0.133	0.178	0.221	0.231
	$1.0h$	U/U_f	0.825	0.833	0.820	0.794	0.753	0.734	0.684	0.669	0.639	0.633
	$1.0h$	V/U_f	0.008	0.016	0.025	0.037	0.051	0.067	0.140	0.186	0.251	0.263
	$2.0h$	U/U_f	0.906	0.905	0.903	0.890	0.864	0.869	0.869	0.876	0.890	0.898
	$2.0h$	V/U_f	0.016	0.028	0.036	0.044	0.067	0.093	0.131	0.166	0.190	0.198
55°	$0.07h$	U/U_f	0.580	0.566	0.548	0.510	0.456	0.394	0.301	0.205	0.000	0.000
	$0.07h$	V/U_f	−0.001	0.002	0.005	0.004	0.006	0.026	0.046	0.070	0.095	0.028
	$0.6h$	U/U_f	0.736	0.731	0.719	0.699	0.655	0.613	0.533	0.478	0.395	0.376
	$0.6h$	V/U_f	0.004	0.010	0.015	0.023	0.027	0.046	0.092	0.115	0.171	0.175
	$1.0h$	U/U_f	0.801	0.796	0.790	0.775	0.745	0.709	0.674	0.655	0.624	0.619
	$1.0h$	V/U_f	0.016	0.018	0.026	0.041	0.049	0.086	0.140	0.191	0.267	0.282
	$2.0h$	U/U_f	0.888	0.889	0.871	0.866	0.854	0.854	0.846	0.858	0.878	0.886
	$2.0h$	V/U_f	0.024	0.027	0.040	0.050	0.071	0.096	0.143	0.173	0.200	0.208
60°	$0.07h$	U/U_f	0.571	0.583	0.564	0.521	0.466	0.399	0.255	0.151	−0.015	−0.006
	$0.07h$	V/U_f	−0.001	0.002	0.003	0.005	0.010	0.010	0.030	0.042	−0.004	−0.007
	$0.6h$	U/U_f	0.739	0.735	0.726	0.691	0.668	0.618	0.533	0.459	0.358	0.340
	$0.6h$	V/U_f	0.004	0.010	0.016	0.027	0.036	0.066	0.110	0.155	0.189	0.197
	$1.0h$	U/U_f	0.821	0.808	0.803	0.779	0.750	0.723	0.671	0.631	0.589	0.581
	$1.0h$	V/U_f	0.007	0.020	0.022	0.032	0.054	0.095	0.156	0.218	0.288	0.309
	$2.0h$	U/U_f	0.894	0.896	0.886	0.875	0.869	0.866	0.868	0.874	0.891	0.900
	$2.0h$	V/U_f	0.020	0.029	0.034	0.047	0.076	0.102	0.151	0.189	0.216	0.223
75°	$0.07h$	U/U_f	0.554	0.540	0.506	0.464	0.411	0.306	0.149	0.034	−0.012	−0.008
	$0.07h$	V/U_f	0.003	0.006	0.010	0.011	0.013	0.019	0.029	0.029	−0.005	−0.004
	$0.6h$	U/U_f	0.719	0.708	0.681	0.660	0.615	0.556	0.443	0.324	0.176	0.144
	$0.6h$	V/U_f	0.011	0.013	0.026	0.030	0.044	0.086	0.150	0.189	0.210	0.198
	$1.0h$	U/U_f	0.798	0.790	0.769	0.744	0.719	0.673	0.605	0.543	0.468	0.454
	$1.0h$	V/U_f	0.020	0.019	0.038	0.043	0.076	0.126	0.213	0.303	0.455	0.494
	$2.0h$	U/U_f	0.891	0.886	0.882	0.862	0.850	0.846	0.848	0.872	0.905	0.917
	$2.0h$	V/U_f	0.029	0.037	0.045	0.065	0.088	0.120	0.190	0.226	0.243	0.253

strongly similar tendency in front of obstacles with a windward slope of 60° or less. The longitudinal (horizontal) velocity began to decrease at a distance of $3.3h$ and reached its minimum at the toe of the stoss slope. Although the decrease began at about the same distance for obstacles with steeper slopes, it reached a minimum at a distance of $0.50h$–$0.74h$, which is likely to indicate the approximate position where the airflow reversed. The increase of velocity between this point and the obstacle, reaching a maximum at $0.275h$, corresponds to the position of the most extreme negative value found in the flow-reversal region in this study.

[17] For all obstacle heights and stoss angles, the vertical velocity (V) increased as the airflow approached the obstacle (Table 1). The acceleration of vertical velocity varied among the heights. An abrupt decrease in vertical velocity, accompanied by downward movement of the flow, occurred near the toe of the stoss slope for obstacles with a stoss angle greater than 60°. This downward movement weakened with increasing height and vanished at a height greater than $0.6h$. As mentioned earlier, the decrease in horizontal velocity that occurs before an obstacle will likely result in the deposition of sand. The direction of the vertical component of velocity will also affect the sand transport processes by altering the direction of the forces exerted on sand particles [*Greeley and Iversen*, 1985]. The upward vertical component at greater distances from an obstacle will increase the lift force and will slow the deposition of moving sand and may even lead to increased entrainment of sand grains on the ground upwind

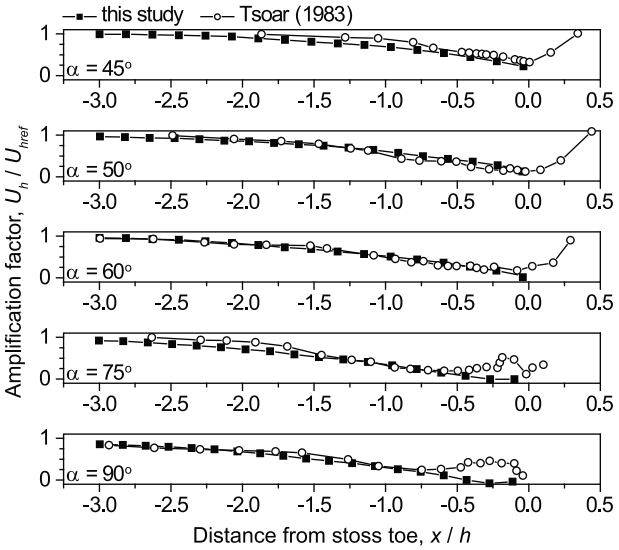

Figure 5. Comparisons of the dimensionless horizontal (this study) and longitudinal [*Tsoar*, 1983] velocities as a function of the distance from obstacles with different stoss slopes; velocities were measured using the PIV in this study and using a hot-wire anemometer in *Tsoar*'s [1983] study. All measured wind velocities are expressed relative to the free-stream wind velocity of 8 m s^{-1} used in this study. All distances above the surface and before and after the model are expressed as multiples of h, the height of the model.

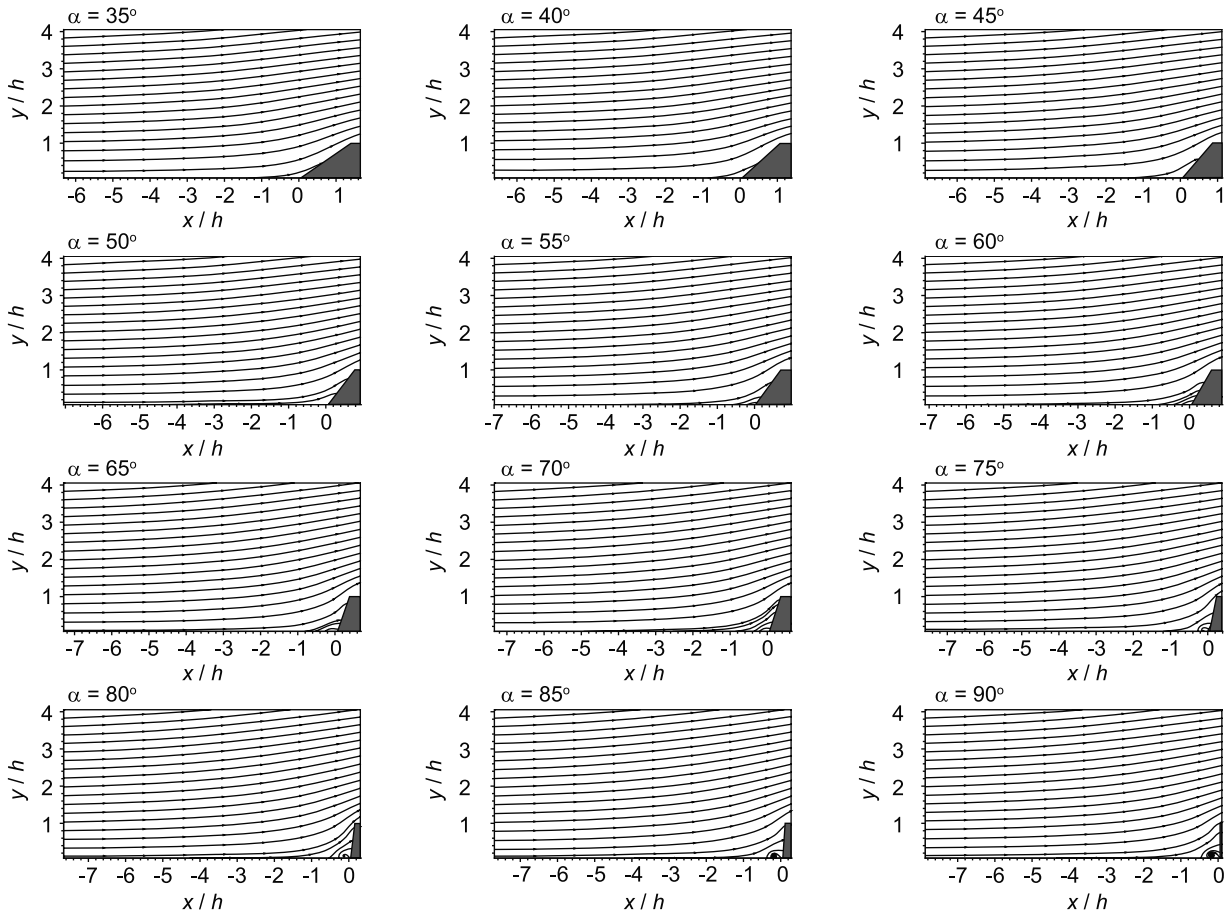

Figure 6. Streamlines upwind of an obstacle as a function of the windward slope. All distances above the surface and before and after the model are expressed as multiples of *h*, the height of the model.

of the obstacle. However, the downward movement near where the reverse vortex forms would combine with the effect of gravitation and decreased horizontal velocity, thereby strengthening the deposition of saltating particles. Therefore, the combined influence of changes in the horizontal and vertical velocities will likely result in the accumulation of sand upwind of a steep obstacle, as *Tsoar* [1983] demonstrated.

3.3. Streamlines and Flow Separation

[18] The streamlines above the windward slope and the flow separation and reattachment in the lee of transverse desert dunes and of coastal foredunes under the influence of offshore winds have been demonstrated by previous studies [*Wiggs et al.*, 1996; *Walker*, 2000; *Dong et al.*, 2007; *Udo et al.*, 2008; *Lynch et al.*, 2009]. These results showed that the development of sand dunes is strongly influenced by the structure of the streamlines as a result of the shear stress exerted on the sand surface; this stress changes as a result of curvature and deformation of the streamlines. Thus, the structure of streamlines upwind of an obstacle will provide clues to the initiation of echo dunes.

[19] Figure 6 reveals two distinctive characteristics of the streamlines upwind of an obstacle: uplift and compression of the streamlines occur when the airflow approaches an obstacle with a windward slope less than 60°, whereas the streamlines undergo separation and subsequently form reversed eddies in front of steeper obstacles. The compression of the streamlines that results from a higher pressure gradient induced by airflow stagnation before the obstacle and the climbing movement of airflow along its windward slope will produce climbing dunes where the stoss slope is less than 60°. In front of steeper obstacles, echo dunes will form where the reverse vortex develops. However, it is difficult to determine the minimum windward slope required for airflow separation by examining the structures of the streamlines because the reverse vortex is likely to be very small under the critical conditions (as can be seen in Figure 6). The reversal of the horizontal velocity occurs in front of an obstacle with a 55° windward slope, but the vertical component has not yet separated at this angle. The disagreement between the critical angles for separation of the horizontal and vertical components indicates that sand accumulation, and consequently the formation of echo dunes in front of such obstacles, will be strongly influenced by both the mean streamlines and the instantaneous velocities.

[20] *Tsoar*'s [1983] wind tunnel simulations of sand accumulation demonstrated that a sand-free area develops in front of an obstacle with a 55° windward slope. His results also suggested that an echo dune would change to a climbing dune after sufficient sand accumulates in front of an obstacle with a 60° windward slope because the deposited sands

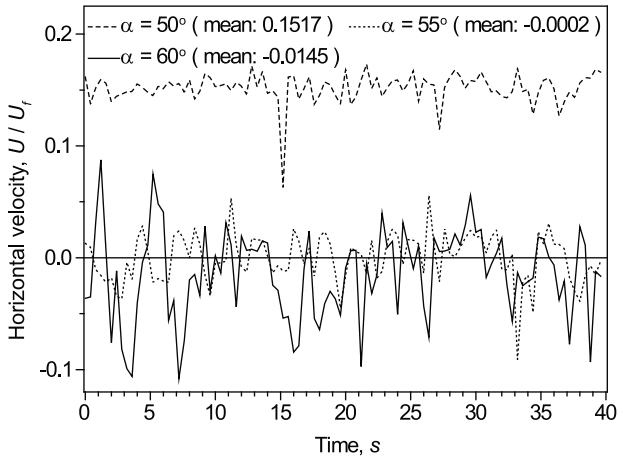

Figure 7. Instantaneous and mean horizontal velocities (U) in front of three obstacles (expressed as a proportion of the free-stream velocity, U_f) showing the critical windward slope angle for airflow separation. Velocities were measured at a distance of $0.1h$ before the obstacles and a height of $0.07h$. All measured wind velocities are expressed relative to the free-stream wind velocity of 8 m s^{-1} used in this study. All distances above the surface and before and after the model are expressed as multiples of h, the height of the model.

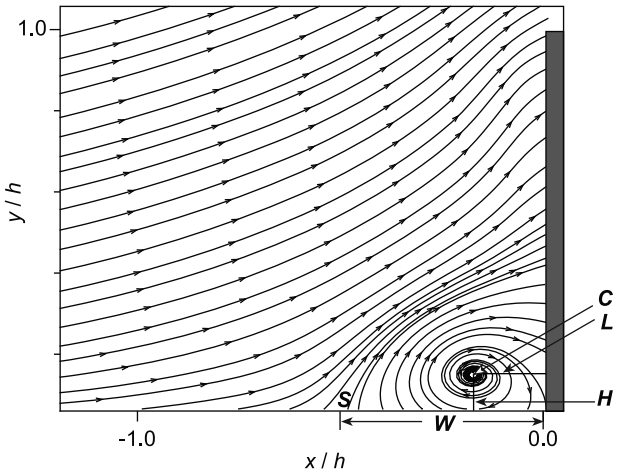

Figure 8. Illustration of the point of airflow separation and the position of the reverse vortex. All distances above the surface and before and after the model are expressed as multiples of h, the height of the model. S, the point of airflow separation; W, the width of the area of reversed airflow, which is defined as the farthest position of the negative horizontal velocity at the lowest height; C, the position of the core of the reverse vortex; L and H, the horizontal distance of the vortex from the obstacle and its vertical height, respectively.

gradually decrease the slope angle. These phenomena imply that the critical windward slope angle for airflow separation and reverse eddy formation should lie between 55° and 60°. Figure 7 shows the instantaneous and mean horizontal velocities that we measured by the PIV at a distance of $0.1h$ in front of the obstacles and at a height of $0.07h$. The velocity fluctuations and average values in front of the obstacles suggest that the minimum windward slope angle for airflow separation is 60°. Although sand could accumulate and form a temporary echo dune before an obstacle with a 55° windward slope, the fluctuation in the structure of the secondary airflow suggests that it will be difficult to sustain the development of echo dunes at this angle.

3.4. Structure of the Reverse Vortex

[21] Figure 8 shows the typical structure of the streamlines and of the reverse vortex. We chose two parameters to characterize the reverse vortex, because the secondary airflow in this region has a significant influence on the initiation of echo dunes. The point of airflow separation (S in Figure 8) can be represented by the width of the region of reversed airflow (W), which is defined as the farthest position of the negative horizontal velocity at the lowest height; the position of the core of the reverse vortex (C in Figure 8) can be represented by the horizontal distance of this position from the obstacle (L) and its height (H) above the surface. These parameters can be calculated from the PIV data. The geomorphological significance of these parameters is that the point of airflow separation (the width of the reversed airflow) corresponds to the stoss slope of the echo dune because notable deposition occurs here, and that the core of the reverse vortex should be related to the position of the dune's crest because the strongest shear stresses occur on both sides of this position.

[22] Figure 9 shows the changes in the distance of airflow separation and the core of the reverse vortex upwind of an obstacle. The width of the region in which airflow separation and reverse flow occur increases linearly with increasing steepness of the windward slope (Figure 9, top). This finding agrees with *Tsoar*'s [1983] results for the positions of sand

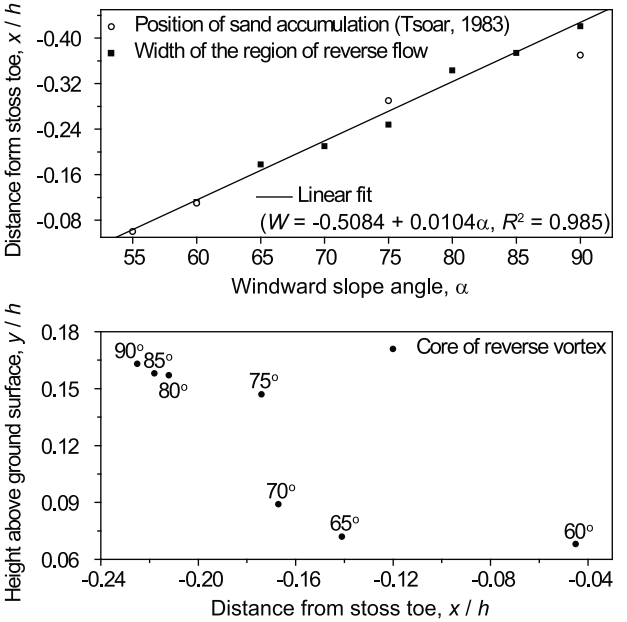

Figure 9. Positions (top) of airflow separation and (bottom) of the core of the reverse vortex upwind of obstacles as a function of the stoss slope angle. All distances above the surface and before and after the model are expressed as multiples of h, the height of the model.

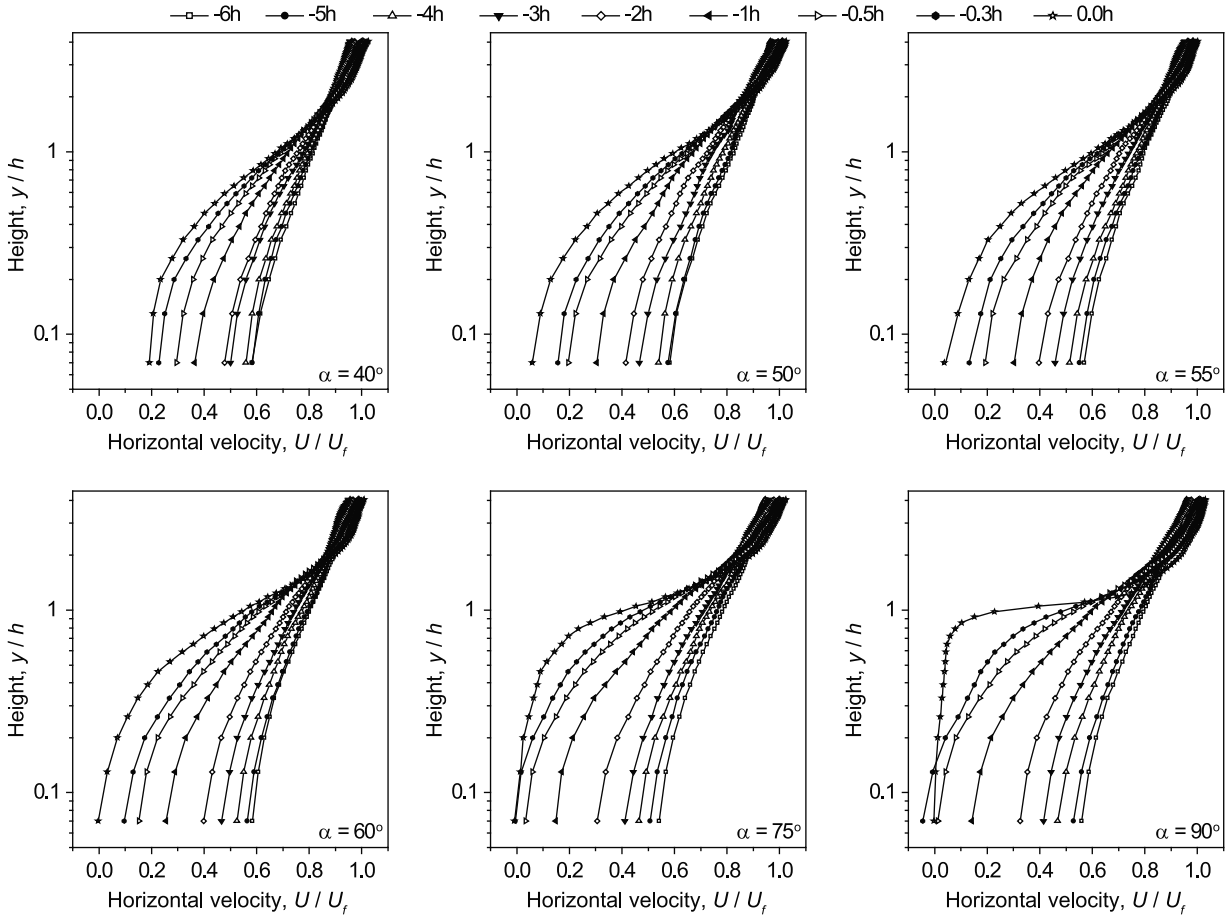

Figure 10. Horizontal velocity (U) profiles in front of obstacles with different windward slopes (expressed as a proportion of the free-stream velocity, U_f). All measured wind velocities are expressed relative to the free-stream wind velocity of 8 m s^{-1} used in this study. All distances above the surface and before and after the obstacle are expressed as multiples of h, the height of the model.

accumulation upwind of obstacles with different stoss angles. The position of the core of the reverse vortex (Figure 9, bottom) shows that the windward slopes can be divided into three groups. For obstacles with a windward slope of 60° or less, the core of the reverse vortex is lowest and closest to the toe of the stoss slope, which suggests that a low echo dune would form here and that its growth would be limited by the height of the reverse vortex. The second group of slopes (between 65° and 75°) is characterized by a rapid increase in the size of the reverse vortex with increasing stoss angle, and the echo dunes that form under these conditions should be larger and farther from the toe of the stoss slope, with both size and distance increasing with increasing slope. The third group includes obstacles with a slope steeper than 75°, which shows a slow increase in the size of the reverse vortex with increasing stoss angle; under these circumstances, the distance of sand accumulation from the obstacle and the height of the echo dune increase only gradually as the windward slope becomes steeper.

3.5. Velocity Profiles and Flow Regions

[23] The horizontal velocity profiles gradually deviated from the "law of the wall," which states that the average velocity is proportional to the logarithm of the distance from the obstacle (Figure 10). This results from the deceleration of wind caused by the presence of the obstacle. The degree of deviation increased with decreasing distance from the toe of the stoss slope and with increasing windward slope angle. The profiles within 2.0h upwind of the obstacles can be divided into three segments: a steep lower segment, a gentle middle segment, and an upper segment characterized by a constant velocity gradient. The inflection points between the lower and the middle segments were located between 0.33h and 0.98h and tended to increase in height with increasing windward slope. The upper inflection points were above the crests of the obstacles and had heights of 1.2h to 2.0h above the surface. The segmented velocity profiles implied that the shear velocity should not be calculated using the slope of the linear wind profile, as has been suggested by previous researchers [*Howard et al.*, 1978; *Mulligan*, 1988; *Wiggs*, 1993; *Frank and Kocurek*, 1994; *Wiggs et al.*, 1996].

[24] The kinks in the velocity profiles have previously been considered to distinguish different airflow regions in the lee of transverse dunes [*Frank and Kocurek*, 1996; *Walker and Nickling*, 2002; *Dong et al.*, 2007]. However, we used the gradient contours of horizontal velocity as a function of height (dU/dy) to distinguish different airflow regions in this study because the segments of the velocity profiles

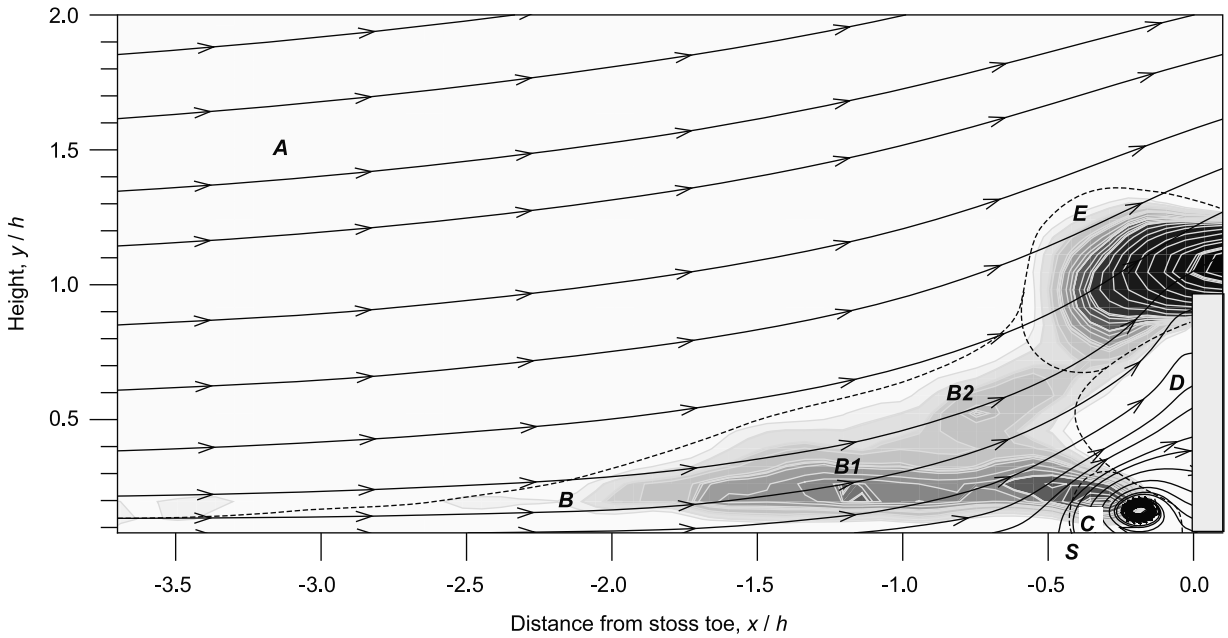

Figure 11. Airflow regions observed in front of a vertical obstacle. A, outer region; B, shear-stress region; C, flow-separation region; D, stagnation region; E, turbulent-shear region. B1 and B2 represent high-shear-stress zones and *S* indicates the point of airflow separation. The contour lines denote the horizontal velocity gradient (d*U*/d*y*). All measured wind velocities are expressed relative to the free-stream wind velocity of 8 m s^{-1} used in this study. All distances above the surface and before and after the model are expressed as multiples of *h*, the height of the model.

transitioned gradually, making differentiation of those segments subjective. On the basis of this parameter (d*U*/d*y*), we distinguished five airflow regions (Figure 11): an outer region (region A), a shear-stress region (region B), a flow-separation region (region C), a stagnation region (region D), and a turbulent-shear region (region E). These regions reflect different degrees of shear stress that result from differences in the characteristics of the secondary airflow pattern.

[25] The outer region (A), proposed by *Jackson and Hunt* [1975] for a low hill with a gentle slope, is characterized by a relatively low velocity gradient and is essentially unaffected by the surface shear forces. The lower edge of this region increased in height as the airflow approached the obstacle because of the effects of deceleration and separation of the airflow. The shear-stress region (B) forms because of friction between the ground surface and the airflow, and shear stress decreases with increasing height in this region. However, two high-shear-stress zones form within this region as a result of airflow deceleration and, consequently, stagnation of the wind near the surface upwind of the obstacle; the lower one (B1, at a height of 0.2*h*) represents the area where the downward airflow collide with the reversed airflow, and the upper one (B2, at a height of 0.5*h*) indicates the area of transition between the undisturbed (A), separated (C), and stagnant (D) airflow in front of the obstacle. The flow-separation region (C) beneath the shear-stress region occupies the area where both the horizontal and vertical velocities reverse; a high-stress zone forms in the upper portion of this region, where the reversed airflow meets the downwind airflow. The stagnation region (D) that forms in front of the obstacle is convex to the upwind direction at a height of 0.5*h* and is concave in both the lower and upper portions; this region is characterized by low wind velocity and a low velocity gradient because of the effect of airflow stagnation. The turbulent-shear region (E) occurs at the top of the obstacle and is the region with the maximum shear stress, which is caused by the abrupt change of topography and consequently the convergence of the streamlines. The shear stress decreased with increasing distance from the obstacle in this region. It is not necessary to distinguish a separate shear-stress region in the upper portions of this region because the turbulent-shear region disappears rapidly with increasing height and blends with the outer region (A).

[26] The boundaries of these regions change as the windward slope becomes gentler, and some regions, such as the separation and stagnation regions, will disappear and a region of uniform shear stress will form when the windward slope angle is less than 60°. The three regions nearest to the ground surface are significant for the formation of echo dunes. As *Tsoar* [1983] indicated, sand deposits start to form at a distance of 2.0*h*–0.4*h* in front of obstacles, which corresponds to the shear-stress region in Figure 11. The sand-free area between 0.3*h* and 0.0*h* in front of the obstacle corresponds to the flow-separation region in Figure 11 and indicates the positions of the crest and the lee slope of the echo dune. The stagnation region in front of an obstacle would create a roll vortex along the trough between the dune and the obstacle, and this phenomenon would account for the sideways movement of sand that has been observed under an equilibrium state for an echo dune [*Tsoar and Blumberg*, 1991]. Moreover, the high stress at B2 in Figure 11 would result in

an unstable state for sands at this distance from the obstacle, and this would indicate the upper limit of the echo dune's height. However, these regions would change as the echo dune evolves, and the effects of the different regions would also subsequently change.

4. Conclusions

[27] We measured the secondary airflow patterns in front of obstacles with various windward slope angles using the PIV in a wind tunnel. The results quantitatively confirmed *Tsoar*'s [1983] findings that the windward slope angle played an important role in determining the patterns of the secondary airflow that developed in front of the obstacles. Horizontal velocities decelerated in front of obstacles with a windward slope angle less than 55°, and reverse eddies formed before the obstacles with a steeper slope. In contrast, vertical velocities increased as the airflow approached the obstacle, and their directions indicated that the minimum windward slope angle at which vertical airflow separation occurs is 60°. The structures of the streamlines and the instantaneous velocities showed that airflow separation (and, consequently, a reverse eddy) formed in front of the obstacles when the windward slope angle was steeper than 60°. This critical windward slope angle for reverse eddy formation agrees with the results of *Tsoar*'s [1983] wind tunnel simulations, which indicated that a stable echo dune formed in front of a solid obstacle with the windward slope of 60° but that a temporary echo dune changed into a climbing dune upwind of a 55° slope.

[28] On the basis of the streamlines, we examined the positions of airflow separation and the structures of the reverse eddies. The distance at which airflow separation occurred increased with increasing windward slope, and there was a strong linear correlation between the width of the region of reversed flow and the position of sand accumulation proposed by *Tsoar* [1983]. However, the position of the core of the reverse eddy moved farther from the obstacle and farther above the ground as the windward slope angle increased. We defined three slope groups based on the position of the reverse vortex and demonstrated the effects of airflow separation on echo dune formation based on these differences.

[29] The horizontal velocity profiles upwind of the obstacles deviated from the law of the wall because of the effects of airflow deceleration and stagnation. We distinguished five airflow regions upwind of an obstacle based on the gradients of horizontal velocity: the outer region, shear-stress region, flow-separation region, stagnation region, and turbulent-shear region. These regions were characterized by different shear effects, and their boundaries would change with changes in the windward slope angle. The positions and characteristics of the shear-stress, flow-separation, and stagnation regions significantly affect sand deposition and the initiation of echo dunes upwind of an obstacle. The positions of the airflow separation and the region of high shear stress define the positions of the crest and lee slope of the echo dune. However, as sand accumulates, the secondary airflow patterns will change and become more complex, and the division of these airflow regions and their effects on the dune should be reconsidered. Additional research will be required to characterize how the relationships observed in this study change as an echo dune forms and begins to evolve.

[30] In this study, we examined two-dimensional secondary airflow patterns in the absence of an actual echo dune, and the airflow approached perpendicular to the obstacles. To adequately simulate a real situation, it will be necessary to monitor airflow patterns in three dimensions, with different angles of incidence for the wind and in the presence of an actual echo dune. In addition to the windward slope, the formation of an echo dune would also be affected by the geometric characteristics of the obstacle (such as its height, length, and angle with respect to the prevailing wind). To resolve this issue, it will be necessary to perform field measurements using more precise techniques, such as using an ultrasonic anemometer, or to conduct numerical modeling (e.g., computational fluid dynamics) based on laboratory or field findings, as in the research performed by *Jackson et al.* [2011]. After all, the initiation and development of echo dunes upwind of obstacles are influenced by complex feedbacks among topography, wind regime, and sand transport, and all of these aspects of their formation will require further research. As our knowledge of these feedbacks improves, it may become possible to develop engineering guidelines for human structures that will avoid or mitigate the impacts of sand accumulation.

[31] **Acknowledgments.** We gratefully acknowledge funding from the National Natural Science Foundation of China (40801007) and the Ph.D. program of the West Light Foundation, Chinese Academy of Sciences (O928631001). We greatly appreciate constructive comments from Derek Jackson, Patrick Hesp, and one anonymous reviewer.

References

Adrian, R. J. (1991), Particle-imaging techniques for experimental fluid mechanics, *Annu. Rev. Fluid Mech.*, *23*, 261–304, doi:10.1146/annurev.fl.23.010191.001401.

Bagnold, R. A. (1941), *The Physics of Blown Sand and Desert Dunes*, 265 pp., Methuen, London.

Bowen, A. J., and D. Lindley (1977), A wind-tunnel investigation of the wind speed and turbulence characteristics close to the ground over various escarpment shapes, *Boundary Layer Meteorol.*, *12*, 259–271, doi:10.1007/BF00121466.

Chojnacki, M., J. E. Moersch, and D. M. Burr (2010), Climbing and falling dunes in Valles Marineris, Mars, *Geophys. Res. Lett.*, *37*, L08201, doi:10.1029/2009GL042263.

Cooke, R. U., A. Warren, and A. Goudie (1993), *Desert Geomorphology*, 526 pp., UCL Press, London.

Dong, Z., G. Quian, W. Luo, H. Wang (2007), A wind tunnel simulation of the effects of stoss slope on the lee airflow pattern over a two-dimensional transverse dune, *J. Geophys. Res. 112*, F03019, doi:10.1029/2006JF000686.

Embleton, C., J. Thornes, and A. Warren (1979), The nature of fluid motion, in *Process in Geomorphology*, edited by C. Embleton and J. Thornes, pp. 39–72, Edward Arnold, London.

Emeis, S., H. Frank, and F. Fiedler (1995), Modification of air flow over an escarpment: Results from the Hjardemal experiment, *Boundary Layer Meteorol.*, *74*, 131–161, doi:10.1007/BF00715714.

Evans, J. R. (1962), Falling and climbing sand dunes in the Cronese ("Cat") Mountain Area, San Bernardino County, California, *J. Geol.*, *70*(1), 107–113, doi:10.1086/626798.

Frank, A., and G. Kocurek (1994), Effects of atmospheric conditions on wind profiles and Aeolian sand transport with an example from White Sands National Monument, *Earth Surf. Processes Landforms*, *19*, 735–745, doi:10.1002/esp.3290190806.

Frank, A., and G. Kocurek (1996), Toward a model of airflow on the lee side of Aeolian dunes, *Sedimentology*, *43*, 451–458, doi:10.1046/j.1365-3091.1996.d01-20.x.

Greeley, R., and J. D. Iversen (1985), *Wind as a Geological Process*, 333 pp., Cambridge Univ. Press, Cambridge, doi:10.1017/CBO9780511573071.

Hesp, P. A., I. J. Walker, S. L. Namikas, R. Davidson-Arnott, B. O. Bauer, and J. Ollerhead (2009), Storm wind flow over a foredune, Prince Edward Island, Canada, *J. Coastal Res., Spec. Issue*, *56*, 312–316.

Howard, A. D. (1985), Interaction of sand transport with topography and local winds in the northern Peruvian coastal desert, in *Proceedings of International Workshop on the Physics of Blown Sand*, edited by O. E. Barndorff-Nielson et al., pp. 377–391, Dep. of Theor. Stat., Univ. of Aarhus, Aarhus, Denmark.

Howard, A. D., J. B. Morton, M. Gad-el-Hak, and D. B. Pierce (1978), Sand transport model of barchan dune equilibrium, *Sedimentology*, *25*, 307–338, doi:10.1111/j.1365-3091.1978.tb00316.x.

Jackson, D. W. T., J. H. M. Beyers, K. Lynch, J. A. G. Cooper, A. C. W. Baas, and I. Delgado-Fernandez I (2011), Investigation of three-dimensional wind flow behaviour over coastal dune morphology under offshore winds using computational fluid dynamics (CFD) and ultrasonic anemometry, *Earth Surf. Processes Landforms*, *36*(8), 1113–1124, doi:10.1002/esp.2139.

Jackson, P. S., and J. C. R. Hunt (1975), Turbulent wind flow over a low hill, *Q. J. R. Meteorol. Soc.*, *101*, 929–955, doi:10.1002/qj.49710143015.

Lancaster, N. (1995), *Geomorphology of Desert Dunes*, 290 pp., Routledge, London, doi:10.4324/9780203413128.

Lancaster, N., and V. P. Tchakerian (1996), Geomorphology and sediments of sand ramps in the Mojave Desert, *Geomorphology*, *17*(1–3), 151–165, doi:10.1016/0169-555X(95)00101-A.

Lancaster, N., W. G. Nickling, and C. K. McKenna Neuman, and V. E. Wyatt (1996), Sediment flux and airflow on the stoss slope of a barchan dune, *Geomorphology*, *17*(1–3), 55–62, doi:10.1016/0169-555X(95)00095-M.

Liu, X. W., S. Li, and J. Y. Shen (1999), Wind tunnel simulation experiment of mountain dunes, *J. Arid Environ.*, *42*(1), 49–59, doi:10.1006/jare.1998.0488.

Livingstone, I., and A. Warren (1996), *Aeolian Geomorphology: An Introduction*, 211 pp., Longman, Harlow, U. K.

Livingstone, I., G. Wiggs, and C. M. Weaver (2007), Geomorphology of desert sand dunes: A review of recent progress, *Earth Sci. Rev.*, *80*(3–4), 239–257, doi:10.1016/j.earscirev.2006.09.004.

Lubitz, W. D., and B. R. White (2007), Wind-tunnel and field investigation of the effect of local wind direction on speed-up over hills, *J. Wind Eng. Ind. Aerodyn.*, *95*(8), 639–661, doi:10.1016/j.jweia.2006.09.001.

Lynch, K., D. W. T. Jackson, and J. A. G. Cooper (2009), Foredune accretion under offshore winds, *Geomorphology*, *105*(1–2), 139–146, doi:10.1016/j.geomorph.2007.12.011.

Mulligan, K. R. (1988), Velocity profiles measured on the windward slope of a transverse dune, *Earth Surf. Processes Landforms*, *13*, 573–582, doi:10.1002/esp.3290130703.

Petrov, M. (1962), Barchan dune and it's formation in desert, in *The Initiation of Desert Landforms and the Methods of Desert Research*, edited by Z. Chen et al., pp. 53–97, Sci. Press, Beijing.

Pye, K., and H. Tsoar (2009), *Aeolian Sand and Sand Dunes*, 458 pp., Springer, Berlin.

Qian, G., Z. Dong, W. Luo, and H. Wang (2009), Variations of horizontal and vertical velocities over two-dimensional transverse dunes: A wind tunnel simulation of the effect of windward slope, *J. Arid Environ.*, *73*, 1109–1116, doi:10.1016/j.jaridenv.2009.06.006.

Raffel, M., C. E. Willert, S. T. Wereley, and J. Kompenhans (2007), *Particle Image Velocimetry: A Practical Guide*, 2nd ed., 448 pp., Springer, Berlin.

Tsoar, H. (1983), Wind tunnel modeling of echo and climbing dunes, in *Eolian Sediments and Processes*, edited by M. E. Brookfield and T. S. Ahlbrandt, pp. 247–259, Elsevier, Amsterdam, doi:10.1016/S0070-4571(08)70798-2.

Tsoar, H., and D. Blumberg (1991), The effect of sea cliffs on inland encroachment of Aeolian sand, *Acta Mech.*, *2*, supplement, 131–146.

Udo, K., Y. Kuriyama, and D. W. T. Jackson (2008), Observations of wind-blown sand under various meteorological conditions at a beach, *J. Geophys. Res.*, *113*, F04008, doi:10.1029/2007JF000936.

Walker, I. J. (1999), Secondary airflow and sediment transport in the lee of a reversing dune, *Earth Surf. Processes Landforms*, *24*(5), 437–448, doi:10.1002/(SICI)1096-9837(199905)24:5<437::AID-ESP999>3.0.CO;2-Z.

Walker, I. J. (2000), Secondary airflow and sediment transport in the lee of transverse dunes, Ph.D. thesis, 257 pp., Univ. of Guelph, Guelph, Ontario, Canada.

Walker, I. J., and W. G. Nickling (2002), Dynamics of secondary airflow and sediment transport over and in the lee of transverse dunes, *Prog. Phys. Geogr.*, *26*(1), 47–75, doi:10.1191/0309133302pp325ra.

Walker, I. J., and W. G. Nickling (2003), Simulation and measurement of surface shear stress over isolated and closely spaced transverse dunes in a wind tunnel, *Earth Surf. Processes Landforms*, *28*, 1111–1124, doi:10.1002/esp.520.

Weng, W. S., P. A. Taylor, and J. L. Walmsley (2000), Guidelines for airflow over complex terrain: Model development, *J. Wind Eng. Ind. Aerodyn.*, *86*(2–3), 169–186, doi:10.1016/S0167-6105(00)00009-X.

White, B. R. (1996), Laboratory simulation of Aeolian sand transport and physical modeling of flow around dunes, *Ann. Arid Zone*, *35*(3), 187–213.

Wiggs, G. F. S. (1993), Desert dune dynamics and the evaluation of shear velocity: An integrated approach, in *The Dynamics and Environmental Context of Aeolian Sedimentary Systems*, edited by K. Pye, pp. 37–46, Geol. Soc., Bath, U. K.

Wiggs, G. F. S. (2001), Desert dune processes and dynamics, *Prog. Phys. Geogr.*, *25*(1), 53–79, doi:10.1177/030913330102500103.

Wiggs, G. F. S., I. Livingstone, and A. Warren (1996), The role of streamline curvature in sand dune dynamics: Evidence from field and wind tunnel measurements, *Geomorphology*, *17*, 29–46, doi:10.1016/0169-555X(95)00093-K.

Z. Dong, J. Lu, W. Luo, and G. Qian, Key Laboratory of Desert and Desertification, Cold and Arid Regions Environmental and Engineering Research Institute, Chinese Academy of Sciences, 320 W. Donggang Rd., Lanzhou, Gansu 730000, China. (gqqian@lzb.ac.cn)